Utilizing deep learning and advanced image processing techniques to investigate the microstructure of a waxy bitumen

Utilizing deep learning and advanced image processing techniques to investigate the microstructure of a waxy bitumen

Navid Hasheminejad [a,*], Georgios Pipintakos [a], Cedric Vuye [a], Thomas De Kerf [b], Taher Ghalandari [a], Johan Blom [a], Wim Van den bergh [a]

[a] *University of Antwerp, EMIB research group, Faculty of Applied Engineering, Groenenborgerlaan 171, Antwerp 2020, Belgium*

[b] *University of Antwerp, Invilab Research Group, Faculty of Applied Engineering, Groenenborgerlaan 171, Antwerp 2020, Belgium*

Abstract

Bitumen, also called asphalt binder, is the key component in asphalt mixtures. Studies to investigate the microstructure of this material show a rich morphology, especially the formation of bee structures in bitumen containing wax. Most research in this field has investigated these microstructures using commercial image processing software that needs a manual selection of these patterns to obtain certain characteristics. This study aims to construct a deep-learning-based object-detection model that can detect these bee patterns in the images acquired from bitumen samples using Confocal Laser Scanning Microscopy (CLSM). The CLSM images are then used to determine the morphological properties of the samples. The properties investigated are some typical roughness parameters and the wavelength calculated by a novel image processing technique based on the two-dimensional fast Fourier transform. In addition, these developed methodologies are used to investigate the influence of short-term and long-term ageing on the microstructure of a waxy bitumen. The results show that the trained deep learning model can be used to successfully detect the location, number, and area of the bee structures. The number of bee patterns and the area of the surface they cover are reduced upon ageing. Furthermore, some strong trends are found between the computed roughness parameters and the ageing level of the samples. Finally, the estimated wavelength of the bee patterns increases by ageing bitumen. The successful development and demonstration of these methods show their great potential in analyzing the microscopic images of bitumen taken by CLSM or atomic force microscopy and the enormous opportunities for future research.

Keywords: Bitumen; Microstructure; Ageing; Confocal laser scanning microscopy; Image analysis; Deep learning

1. Introduction

Among the different products of crude oil distillation, bitumen, also known as asphalt binder, possesses a dominant role in road and roofing applications due to its superb binding and waterproofing performance [1].

Although bitumen serves its purpose well as a viscoelastic material in road applications, the complexity of its composition made bitumen's overall unmasking a point of consideration already for a long time [2]. Additionally, the organic nature of bitumen hinders the understanding of its fundamentals since it makes it prone to oxidation [3], with several physicochemical alterations taking place [4,5]. The latter is a phenomenon widely known as the ageing of bitumen, taking place in a two-stage fashion, namely during production and paving stages and later in-situ [6,7]. It is reasonable that many studies have focused on the consequences of this process in bitumen, since it's the binding medium of asphalt and inevitably affects its performance with undesirable distresses. To name some of the most severe distress types, cracking and ravelling of asphalt are in the top list [8,9].

Not only the phenomenological behavior and chemical mechanisms of bitumen have received special attention but also the understanding of its interior labyrinth has generated much interest in the scientific community. Different theories concerning bitumen's microstructure have been put forward, varying from a colloidal structure [10], to a dispersed fluid [11], to a modern agglomeration of the most polar bitumen constituents [12]. To reveal intrinsic information in the bulk of bitumen i.e. with respect to aromatic associations and their size, advanced tools are required, such as Small-Angle Neutron and X-Ray Scattering [13]. In addition, limited studies performing measurements in the bulk of bitumen showed that bitumen structures appear only on the surface and can reappear after reheating the fractured specimen representing the bulk [14–16]. The reliability of the surface microstructural patterns and their correlation with binder's properties can in principle be valid since such structures can reappear upon heating of fractured specimens representing the bulk of the bitumen. Hence, a more simplistic approach being adopted more commonly is to understand, as a first step, changes that are depicted on bitumen's surface or subsurface. An ally to achieve this goal is the improvement of microscopic techniques during the last decades [17–19]. Different microscopic techniques have been used to see the annealing effects, the influence of thermal history as well as the effect of ageing on the surface microstructure of bitumen. Until now, Atomic Force Microscopy (AFM) has been proven one of the best candidates for such purposes [20–22] mainly due to its excellent resolution and the relatively undamaged surface after the measurements. Recently, the enhancement of Confocal Laser Scanning Microscopy (CLSM) in reflectance mode has resulted in resolution comparable to the AFM [23].

It has also been speculated that one of the main surface microstructural patterns that AFM can capture is related to one of the components of bitumen. These patterns have been established in the bitumen terminology as ‘bees’ since they were initially visualized in AFM as wrinkled bee-shaped structures [24]. Recently, these bee patterns have been reported to be observable by CLSM as well [23]. In parallel, strong debate existed regarding the origin of these bee patterns. Despite the widespread belief that these surface structures may be associated with the most polar constituents of bitumen known as asphaltenes [25], undeniable evidence was later provided by Differential Scanning Calorimetry (DSC), coupling the bee structures with the paraffinic wax present in bitumen’s composition [26,27]. Although natural wax is not apparent in all bitumen, when present, it may affect the performance of the waxy binders [28,29]. Thus, understanding the influence of waxes is essential for drawing certain conclusions in the effort to understand bitumen’s composition as well as the way to intervene with appropriate modifications or antiageing agents.

Previous research tended to focus on the effect of ageing on the bee patterns investigating the surface of bitumen after artificial ageing in the lab. Commonly, the short-term ageing up to the paving stage is simulated in the lab with the Rolling Thin-Film Oven Test (RTFOT) [30], while the long-term ageing in service with the Pressurised Ageing Vessel (PAV) [31]. Challenges mainly arise concerning the convergence of the findings of different scholars when it comes to the influence of ageing in the area or the length of the bee patterns [32–34], whereas a few have reported the effect of ageing on other characteristics of the bees [35]. For the detection of these patterns, most of the studies have used commercial software packages which need a manual selection of the bees and have their limitations in terms of correct selection of the bee areas.

What is still missing from the literature is a comprehensive study utilizing advanced image processing and deep-learning algorithms. To that end, this study exploits some novel techniques on images acquired by a CLSM to analyze the effect of ageing after laboratory short- and long-term ageing for a waxy bitumen. In contrary to previous works, this paper makes use of a deep learning technique [36] to detect the location of the bee structures to investigate their surface roughness and proposes a new method based on two-dimensional fast Fourier transform (2-D FFT) [37] to identify in the most precise way the wavy characteristics of the bee structures. The analysis adds

to the existing literature a versatile image detection algorithm and serves towards overcoming a longstanding challenge with respect to the true impact of ageing on the bee structures. Finally, it describes the framework of the developed MATLAB algorithm in order to be reproducible by other researchers.

2. Materials and methods

2.1. Bitumen and ageing simulations

Based on previous studies stressing the association of the formed bee patterns with paraffinic wax, a bitumen containing natural wax (crystallizable compounds) was selected. The unaged material was designated in the following as 'waxy bitumen' with the empirical properties and its performance grade provided in Table 1. It is worth mentioning that the selected bitumen was indicated to contain natural wax as was shown by its melting enthalpy calculated via DSC measurements, while wax-free bitumens present a melting enthalpy after heating/cooling DSC cycles of zero. With regard to the refinery process, the specific bitumen is produced after a visbreaking process which among others targets to reduce the viscosity of bitumen.

Table 1: Empirical and wax properties of waxy bitumen

Waxy bitumen	Property		Protocol
	Penetration 25 ºC (0.1 mm)	190	EN1426
	Softening point (ºC)	39.2	EN1427
	Penetration index, PI	-0.63	EN12591
	Performance grade	52-22	AASHTO MP 1
	Melting enthalpy (J/g)	9.6	[29]

The waxy bitumen was aged in the lab for short-term ageing with RTFOT and long-term ageing with PAV according to the European standards [30,31]. Typically for the simulation of short-term ageing 35 grams of unaged material are poured in appropriate flasks after which they are placed in a rotating carousel at 163 °C and flushed with an airflow of 4 L/min for 75 minutes. To mimic the long-term ageing 50 grams of short-term aged material are placed on metallic pans in a chamber under a pressure of 2.1 MPa at 100 ºC for 20 hours. Finally, to distinguish between the different ageing states the nomenclature of 'RTFOT' or 'PAV' will follow the binder designation.

2.2. Sample preparation

The microstructural properties of bitumen are strongly dependent on its thermal history. That is why sample preparation is a critical step in investigating bitumen using any type of microscopy. In this study, the samples preparation recommended by [38] was adopted to conduct the experiments. This procedure includes heating a small portion of bitumen for 30 min at 150 °C followed by a proper stirring to obtain a homogenous material. Then a drop of the material is placed on a microscopic slide placed horizontally on a heating plate at a temperature of 150 °C. The microscopic slide is kept on the heating plate for 1 min to acquire a flat sample with sufficient thickness and a smooth surface. Finally, the sample is placed in a dust-free and dark environment for two hours to cool down to ambient temperature before the CLSM images are taken.

2.3. Microscopic observation and surface characterizations

The microscope used in this study was a Keyence CLSM with a VK-X1000 controller unit and a VK-X1050 measurement head coupled with a Nikon EPI Plan Apo 150X lens. This microscope has a lateral resolution of 5 nm and axial resolution of 10 nm in the best conditions. The microscope uses two light sources. Laser light with a wavelength of 661 nm that scans the surface in the X, Y, and Z direction to capture the image containing the height information and white light to capture the color information from the sample surface. Moreover, a pinhole confocal optical system is used to eliminate all influences of ambient light and reflected light from any position other than the focal point.

The images were taken with the VK-Viewer software and preprocessed using the VK-MultiFileAnalyzer software. The data recorded by the VK-Viewer that were used in this study were the height information of the sample surface and the images produced with the Differential Interference Contrast (DIC) imaging method. The preprocessing of the data with VK-MultiFileAnalyzer included a reference plane setting to level the surface and a surface shape correction using waveform removal with a correction strength of 5 to remove the curvature of the bitumen drop. Afterwards, the DIC images and the height measurements were exported to MATLAB for further analysis.

2.4. Surface roughness evaluation

One advantage of CLSM to other microscopy techniques is its ability to provide high-resolution height measurements from the surface of the specimens. Using these height measurements, it is possible to calculate different surface roughness parameters of the samples at different conditions and compare the microstructures. In this research, five popular surface roughness parameters from the amplitude parameter group were calculated that can help quantify the changes in the height of the surface and explore the observed patterns. These parameters include arithmetic average height (S_a), root mean square height (S_q), maximum height (S_z), skewness (S_{sk}), and kurtosis (S_{ku}), see Equations 1-4.

Arithmetic average height (S_a), also known as the center line average, is the most typical roughness parameter used for general surface control. S_a expresses the differences in the height of each point compared to the arithmetical mean of the surface and is calculated according to Equation 1:

$$S_a = \frac{1}{A} \iint_A |Z(x,y)| dxdy \qquad \text{Equation 1}$$

with Z(x,y) the height of the surface at a point with x and y coordinates, and A the area of the investigated surface.

Root mean square height (S_q) is the standard deviation of the distribution of the surface heights, calculated according to Equation 2. This parameter which describes the surface roughness using statistical methods is similar to S_a but more sensitive to large deviations from the mean line.

$$S_q = \sqrt{\frac{1}{A} \iint_A Z^2(x,y) dxdy} \qquad \text{Equation 2}$$

Maximum height (S_z) is defined as the sum of the largest peak height and the largest pit depth in the designated area.

Skewness (S_{sk}), calculated using Equation 3, is a value that represents the degree of bias of the roughness shape. This parameter is sensitive to occasional deep valleys or high peaks. S_{sk} near zero points out symmetrical height

distribution around the mean plane. Negative or positive values of S_{sk} mean the height distribution is skewed above or below the mean plane.

$$S_{sk} = \frac{1}{{S_q}^3}\left[\frac{1}{A}\iint_A Z^3(x,y)dxdy\right] \quad \text{Equation 3}$$

Kurtosis (S_{ku}) is the fourth central moment of profile amplitude probability density function, computed using Equation 4. This value is representative of the sharpness of the probability density.

$$S_{ku} = \frac{1}{{S_q}^4}\left[\frac{1}{A}\iint_A Z^4(x,y)dxdy\right] \quad \text{Equation 4}$$

S_{sk} and S_{ku} are typically used to differentiate between surfaces that have different shapes but similar values of S_a.

In this research, these values are calculated at four different random locations for each sample, and the average and standard deviation of the computed values are presented.

2.5. Pattern detection using deep learning

Deep learning is a popular computational method that enables computers to learn from experience. Deep learning is a subset of machine learning that uses a hierarchical artificial neural network to carry out the desired tasks. This powerful technique has dramatically improved the state-of-the-art in many domains such as speech recognition, visual object recognition, and object detection [39]. In this research, deep learning was used to detect the so-called “bee patterns” on the surface of the bitumen microstructure. Several deep learning techniques exist for object detection purposes, including Region-based Convolutional Neural Network (R-CNN) [40], Fast R-CNN [41], Faster R-CNN [42], You Only Look Once (YOLO) [36] version 1 to 5, Single Shot Detector (SSD) [43], and EfficientDet [44]. In this study, a YOLOv3 [36] based algorithm developed in the MATLAB environment was trained and used. Contrary to many other methods, YOLOv3 applies a single neural network to the full image, and by dividing the image into multiple regions, it predicts bounding boxes and their probabilities for each region. These bounding boxes are weighted by the predicted probabilities.

As presented in Figure 1, the deep learning network structure in this research consists of the feature extraction network in SqueezeNet, followed by two detection heads at the end, with the second detection head able to detect smaller patterns. The resolutions of the input RGB images for the network were chosen 277*277, and all the images and the bounding boxes were resized accordingly. Next, with the help of the estimateAnchorBoxes function of MATLAB, the number of anchor boxes was selected equal to six, with the three larger ones used in the first detection head and the smaller ones assigned to the second detection head. Anchor boxes are a set of predefined bounding boxes of a certain height and width that can help improve the speed and efficiency of the detection portion of the network. Finally, the system was trained on GPU of a laptop with Intel Core(TM) i7-9850H with a clock speed of 2.60 GHz, 32.0 GB RAM, and a GPU of NVIDIA GeForce MX150.

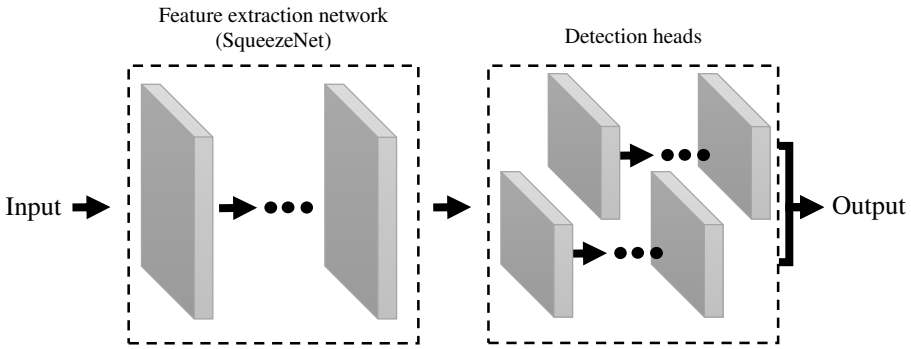

Figure 1: Flow chart of the deep learning network

In this research, first, the bee patterns on 21 images were labeled using the Image Labeler application of MATLAB (see Figure 2-a). Each of these images had between 4 to 13 visible bee patterns. The images used for this purpose were the DIC images taken with the microscope and preprocessed using the VK-MultiFileAnalyzer software. Afterwards, using a data augmentation procedure including random rotation, up to 10% scaling of the images, and color jitter (with no saturation), the number of labeled patterns was increased. One example of an augmented image created using Figure 2-a is presented in Figure 2-b. This increases the variety of the training data, which can improve the accuracy of the trained network. The trained network was eventually able to automatically

detect the bee patterns in the pictures acquired by the CLSM as presented in Figure 2-c and limit the user bias only to the labeling stage.

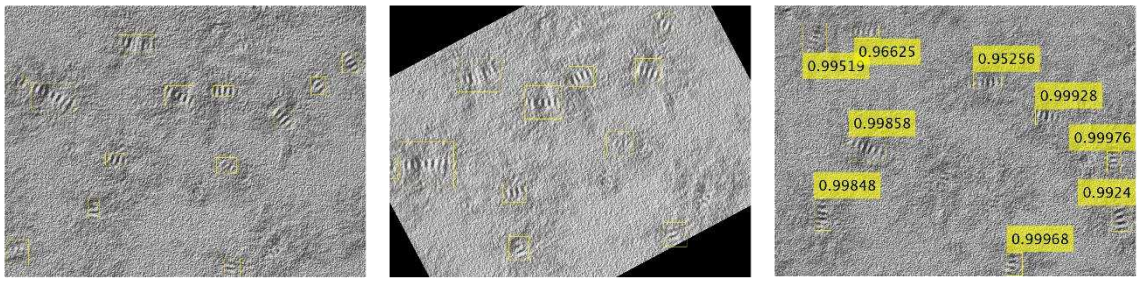

[a] [b] [c]

Figure 2: a) An example of a labeled image, b) Example of an augmented image, and c) Detected bee patterns from the trained algorithms including the certainty of detection

The trained algorithm was then run for all the images captured from the bitumen surfaces detecting the present bee patterns. After detecting the bee patterns, the number and the area of the bounding boxes in each image were calculated and compared for bitumen in different ageing stages.

2.6. Analysis of the patterns by developing advanced image processing techniques

The next step after pattern detection is to identify some characteristics of these bee patterns to investigate if any change can be observed between the microstructure of the samples at different ageing stages. The first parameters calculated for this purpose were the surface roughness parameters such as S_a, S_q, and S_z. To calculate these parameters, the locations of the bees were detected on the DIC images using the trained deep learning algorithm, and the corresponding areas in the height images taken by the CLSM were marked (see Figure 3). Then using Equation 1 and Equation 2, the desired roughness parameters were calculated, and their averages were compared between different samples.

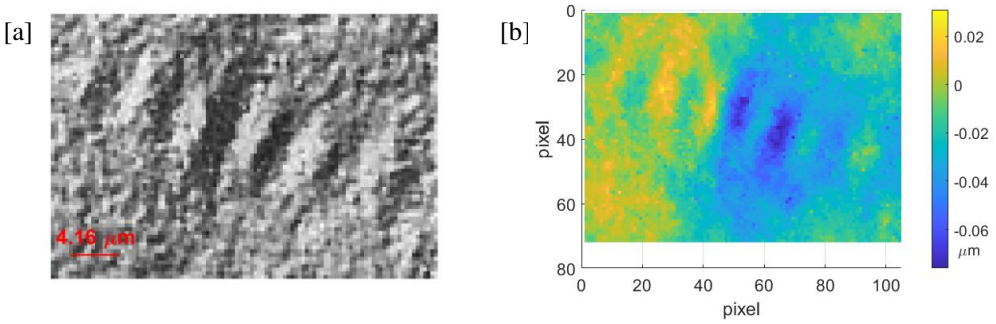

Figure 3: [a] DIC image, and [b] height measurements of a single detected bee from the deep learning algorithm

Another interesting parameter of these patterns is the distance between two consecutive heights called the wavelength (λ). In the literature, this parameter is calculated by drawing a line along with the bee pattern and measuring the distance manually using any image processing software [16,45]. However, this method to estimate the wavelength is time-consuming and susceptible to human error. To automate this process and conduct it for all the bee patterns detected in all images, it is first necessary to develop a method that can estimate the orientation of a bee pattern (angle of the axis of the bee pattern with respect to the x-axis) in an image. This was done by developing an algorithm based on 2D-FFT. 2D-FFT in digital image processing is a tool allowing to decompose an image into its sine and cosine components. The output of this transformation represents the image in the frequency domain. Equation 5 shows the process of calculating 2D-FFT for an image f(x,y) in spatial domain with dimensions of M*N pixels [46].

$$F(u,v) = \sum_{x=0}^{M-1}\sum_{y=0}^{N-1} f(x,y).e^{-j2\pi(\frac{ux}{M}+\frac{vy}{N})} \qquad \text{Equation 5}$$

with F(u,v) the image in the frequency domain.

2D FFT is an efficient and popular method to remove periodic noise from digital images [46]. After applying a 2D FFT on an image and plotting the magnitude of the output in the logarithmic scale in Figure 4-a, two spots with higher values along the direction of the bee pattern are clearly visible. All the main frequency contributors to this image in all directions were found by calculating the radially averaged power spectrum (see Figure 4-b). However, using this figure, it is not possible to obtain the main frequency contributing to the bee pattern in the desired

direction. Therefore it is first necessary to find the direction of the bee pattern in an image. To find the direction of a bee pattern in the image, first, the image was rotated from 0 to 180 degrees. The averages of the spectrum of the middle 22 pixels (selected based on the range of the bee dimensions) on the x-axis were calculated for each rotation angle (see Figure 4-c). The maximum value, 16º for this image, shows the direction of the bee pattern for this example.

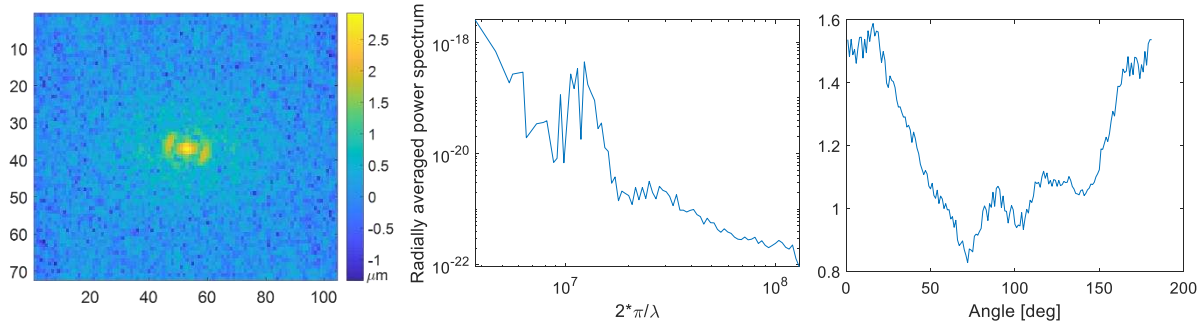

Figure 4: a) Image of Figure 3-b in frequency domain (magnitude of the 2D FFT), b) Radially average power spectrum of this image, and c) Average of the middle 22 pixel values on the x-axis of the spectrum image rotated between 0 to 180 degrees.

After the bee pattern was rotated at an angle of 16° (shown in Figure 5-a), the values along the axis of the pattern were selected. Then, the spectrum of this height data was calculated using a 1D-FFT (see Figure 5-b). The maximum value of this figure in the expected region provides the dominant frequency and, consequently, this pattern's wavelength. However, to make sure the zero values caused by the rotation of the image in MATLAB do not influence the spectrum, a hamming window was first applied to the pattern. The result of the FFT (spectrum) for this bee pattern is presented in Figure 5-b. By reversing the x-value at this peak, the wavelength of this bee pattern was estimated. Using this developed methodology, the wavelength of all detected bee patterns in all images were estimated and compared for bitumen with different ageing severity.

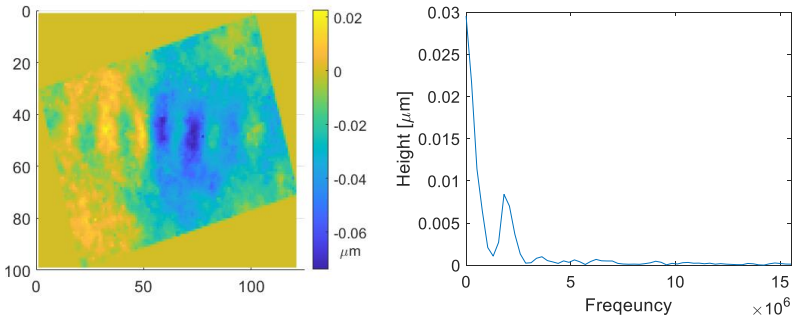

[a] [b]

Figure 5: a) Height measurements of the detected bee pattern rotated to the horizontal position, b) Spectrum of the bee pattern along the x-axis after applying a Hamming window in time domain

3. Results and discussion

The DIC images and height measurements acquired by the CLSM on one location of each sample are presented in Figure 6. A bee structure similar to the ones observed in the literature is present in the microstructure of all three specimens. The number of this pattern seems to decrease in the PAV aged sample, but instead, some larger wrinkles are formed around the remaining bee structures. To study these images systematically, the proposed methodologies explained in the previous section were employed, and multiple microscopic images from each sample were analyzed. The results of this investigation are presented in the following subsections.

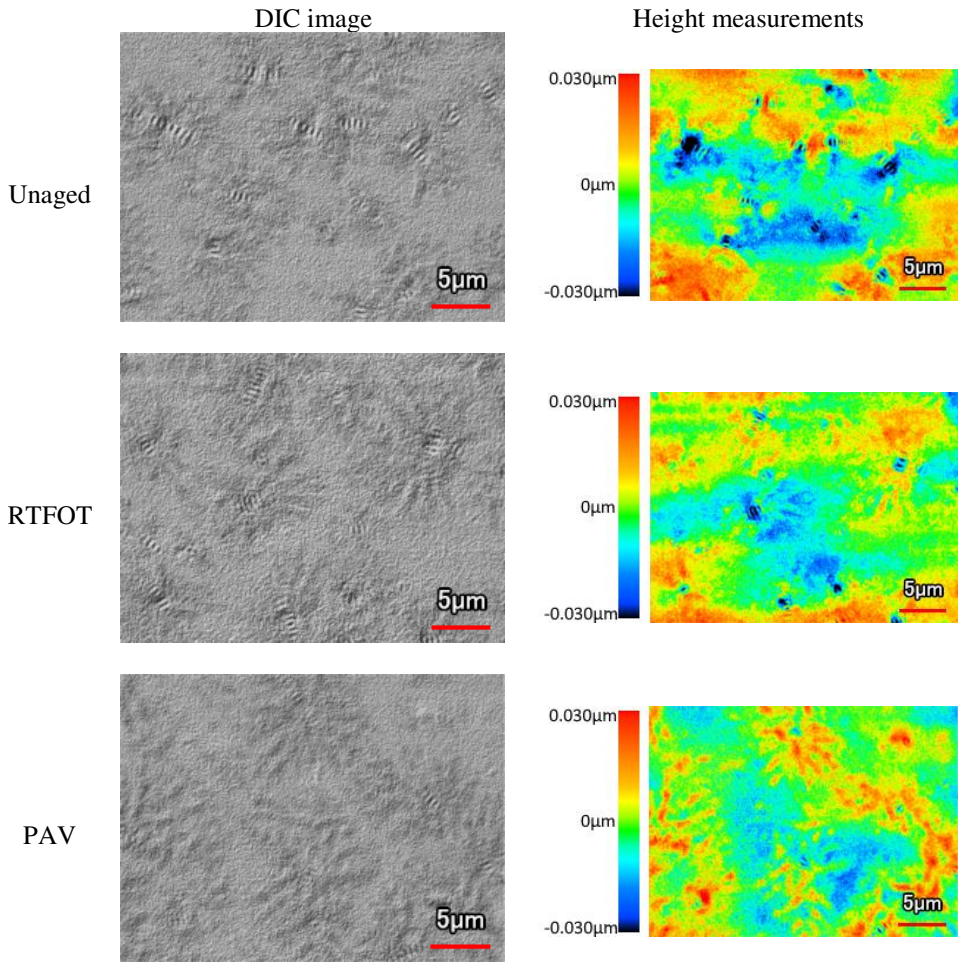

Figure 6: DIC images (left) and height measurements (right) acquired by the CLSM for the bitumen sample in three different ageing stages

3.1. Overall surface roughness

Average and standard deviation of different surface roughness parameters computed for four random locations on the surface of the three samples are presented in Figure 7 and Figure 8. These parameters were calculated for the whole measured areas and present information about the entire measured surfaces and not only the bee patterns. It can be seen that S_a and S_q did not follow a certain trend by ageing. This shows that the differences in the height of each point compared to the arithmetical mean of the surface are not sensitive to the ageing state of the bitumen. However, as it can be seen in Figure 7-c, S_z had a gradual decrease from more than 0.1 µm for the unaged sample to 0.92 µm and 0.08 µm for the RTFOT aged and PAV aged samples, respectively. This means that the difference between the peak height and the largest valley depth of the surface had a gradual decrease by ageing the sample.

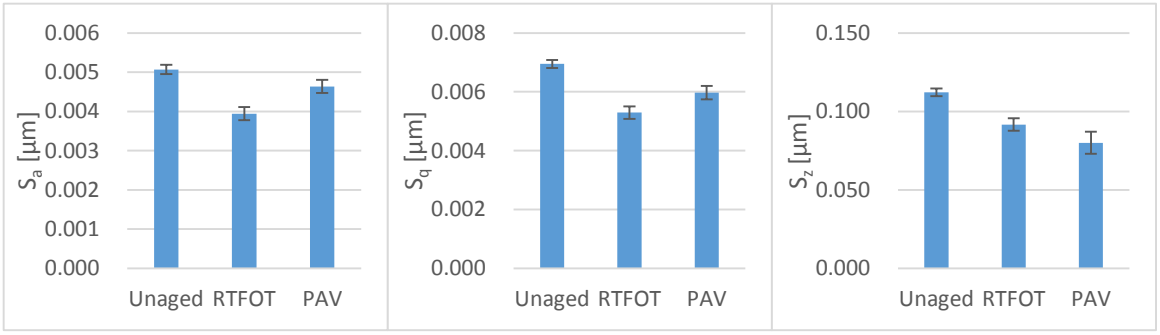

[a] [b] [c]

Figure 7: a) Arithmetic average height, b) root mean square height, and c) maximum height of bitumen surface at different ageing states

Since S_a and S_q do not follow a specific trend in the samples, S_{sk} and S_{ku} are calculated. Figure 8-a shows that S_{sk} changes from less than -0.6 for the unaged state to about -0.48 for the RTFOT state and dramatically increases to more than 0.2 after PAV. This means that the height distribution on the surface of the samples is skewed above the mean plane in the unaged and RTFOT samples, but skewed below the mean plane for the PAV sample. This increasing trend hints that the surface contains fewer valleys and more peaks after the ageing procedures.

Figure 8-b illustrates the kurtosis of the samples. The relatively high kurtosis (S_{ku} > 3) in all samples suggests there are quite some sharp peaks and valleys in these surfaces. This value has a slight decline by RTFOT ageing, and a rather sharp drop in the PAV aged sample, confirming the changes in S_{sk}.

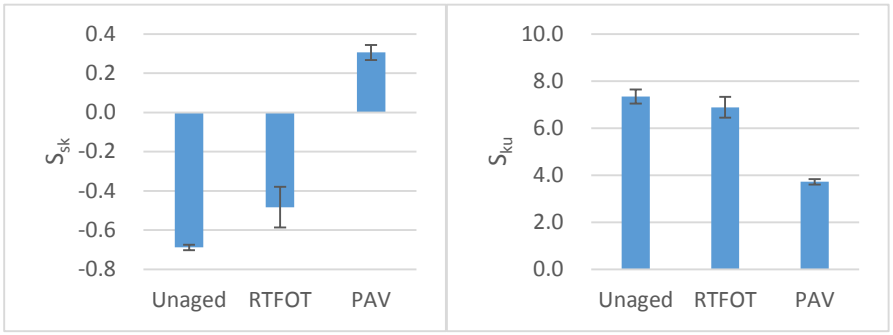

[a] [b]

Figure 8: Skewness and kurtosis of the surface height measurements

3.2. Bee detection

Next, the trained deep learning algorithm was utilized to detect the bee patterns in all the acquired images. After detection of the patterns, their number, size, and the total area they cover in an image were computed and presented in Figure 9. As it can be observed in this figure, the number of the bee patterns in an area of 24.3*32.4 µm decreased by ageing the bitumen. This confirms the initial observations made in Figure 6. Furthermore, the average rectangular area of the bee patterns had a slight decrease with ageing. However, the standard deviation of this parameter is too large to draw any concrete conclusions. Finally, the total areas the bee patterns are covering (Figure 9-c) decreased from more than 50 µm^2 for the unaged state to about 37 µm^2 for the RTFOT stare and less than 20 µm^2 after PAV. These values also had rather large standard deviations, which means even though the area that the bee patterns cover clearly declines by ageing, their density at different locations of the samples varies drastically. These observations can be linked with the crystallization phenomena in waxy bitumen. Since bitumen is considered to be affected from a chemical perspective by oxidation, it has been speculated that the compatibility of the waxes in the bitumen matrix is possible to alter with ageing. Waxes are considered in general unaffected by ageing, however, their compatibility in the bitumen matrix can, in principle, affect the melting point depression

and crystallization temperatures [47,48]. As such, the shift of the crystallization temperatures due to ageing may be a factor for these microstructural changes and the accompanying properties extracted with deep-learning for CLSM. The simultaneous restricted mobility of bitumen due to an increase in its viscosity with ageing may also influence the time-dependent crystallization and, therefore, microstructure. Finally, in another study, it has been shown, with high-resolution Time of Flight Secondary Ion Mass Spectrometry images, that the same waxy bitumen, used in this study, appeared to reduce the aliphatic fragments associated with waxes upon ageing [7]. This can be another reason for the reduction of the number and size of the bee structures, as observed in this paper.

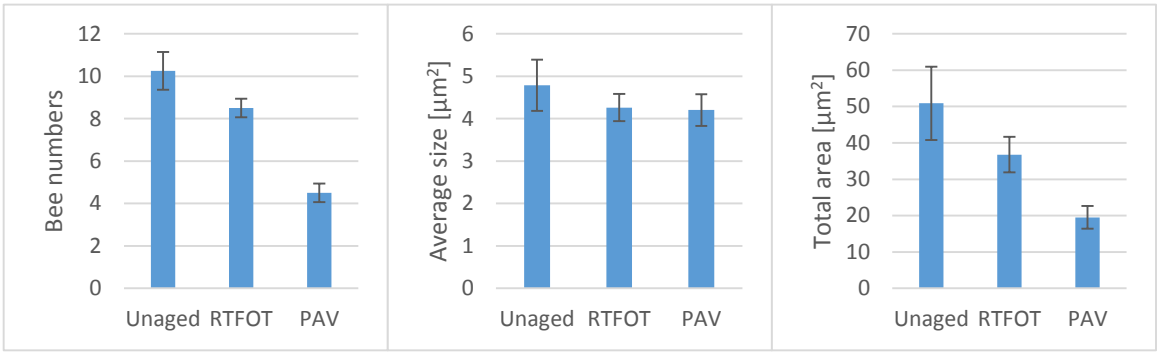

Figure 9: a) Number of detected bees using the developed deep learning algorithm, b) averaged area of the estimated bounding boxes, and c) total area of the patterns on the surface of an image

3.3. Properties of the bee patterns

The roughness parameters calculated in subsection 3.1 represent not only the bee patterns but also the rest of the microstructures formed on the surface. In this subsection, about 100 detected bee patterns in 12 microscopic images taken from the three samples are separated and investigated without taking into account the rest of the surfaces. Figure 10 illustrates three roughness parameters S_a, S_q, and S_z. As it can be seen, S_a, S_q, and S_z of the bee patterns detected on the unaged sample are considerably larger than those of the other two samples. This proves that the bee patterns of the unaged sample are rougher and have higher peaks and valleys with respect to the other two samples. As for the comparison between the aged samples, the Sa values are too close to each other, and the standard deviations are too high to draw any conclusions. However, S_z and S_q which are more sensitive to large deviations

from the mean line than S_a, have a slight decrease in the case of the PAV aged sample with respect to the RTFOT aged sample. Studying Figure 7 and Figure 10 together, it can be concluded that the wrinkles and structures other than the bee patterns are also playing a considerable role in the surface roughness of the samples.

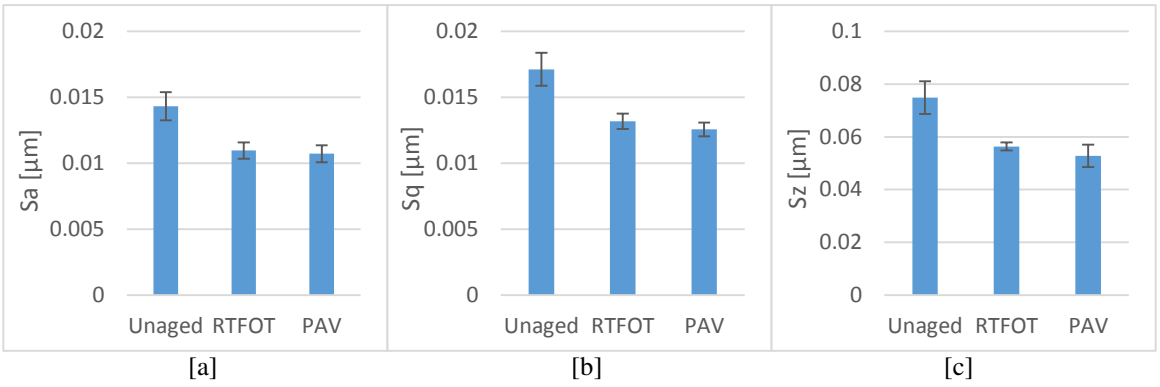

Figure 10: Roughness parameters S_a, S_q, and S_z calculated only in the areas with detected bee patterns

Another approach to evaluate the patterns on the surface of the specimen is a comparison between the wavelength of the bee patterns. At this step, the novel method introduced in subsection 2.5 was used to estimate the wavelength of about 100 bee patterns in the acquired images. The results of this analysis are presented in Figure 11. In this figure, the horizontal lines inside the boxes show the mean values of the data, and the X marks on top of the lines show the median values (second quartile). Furthermore, the top of each box represents the third quartile, while the bottom of the box represents the first quartile. Moreover, the top and bottom lines, also referred to as the whiskers, indicate the variability outside the upper and lower quartiles. As illustrated in this figure, the mean and median wavelength of the bee patterns has a slight increase by RTFOT ageing, and a strong rise by PAV ageing. However, the interquartile range and variability of the data points are quite extensive for all three samples, especially for the PAV-aged sample. The values of the wavelength achieved by this method are comparable with the results of the wavelength of different types of bitumen found in the literature (0.560 µm in [16] and 0.550 µm in [45]).

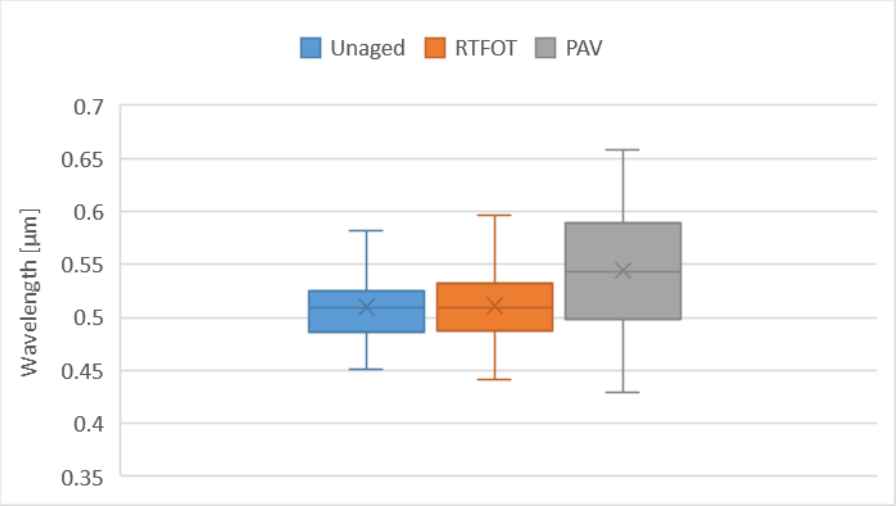

Figure 11: Wavelength of the bee patterns calculated using the proposed method

4. Conclusions

While studies to observe the microstructure of waxy bitumen are available in the literature, a systematic analysis of the number of bees, their dimensions, and characteristics is still missing. In this study, some advanced image processing techniques are developed to detect and analyze the bee structures of a bituminous binder at three different ageing states: Unaged, RTFOT aged, and PAV aged. First, using the trained deep learning model the bee patterns are successfully detected in the images taken by the CLSM. Then, different characteristics of the surface and bee patterns are calculated and interesting trends between these parameters and ageing of bitumen samples are found. The main findings of this study are as follows:

- The CLSM measurements on the bitumen surface show the bee structure similar to what has been observed in the literature (mostly by AFM). The observed bee structures vary in size, density, and surface properties.
- By training a deep learning neural network model, these bee patterns can be detected in the microscopic images limiting the user bias only to the training step.

- Using the height information recorded by the CLSM, multiple roughness parameters can be computed for the surface of the samples or on the regions of the detected bee patterns separately.
- The novel method based on 2D-FFT proposed in this research can estimate the wavelength of the bee structures. This provides the possibility to easily study this parameter for a large number of bee patterns.
- By increasing the ageing level of bitumen, the S_z and S_{ku} parameters decrease while S_{sk} rises. This indicates the surface has a smaller maximum height and kurtosis, and larger skewness upon ageing the bitumen.
- The number of bee patterns, their total area, and roughness parameters S_a, S_q, and S_z go down by ageing the bitumen sample. The decrease in these roughness parameters means that the bee patterns get smoother by ageing the bitumen. Furthermore, even though the variation of the wavelength of the bee patterns is very high, its average increases by ageing the bitumen sample.

The novel methods proposed and employed in this research can radically advance the analysis of the microstructure of the bitumen to establish a correlation between these patterns and other properties of bitumen. Since the methods proposed in this study proved to be capable of analyzing the bee patterns and their properties, it is recommended that other researchers dealing with the microstructure of the bitumen use similar techniques. Future research must focus on using these techniques to analyze more types of bitumen and their microstructure after ageing, the effect of different types of wax on the microstructure of the bitumen, a comprehensive study on the relationship between the bee characteristics and chemical and rheological properties of bitumen, and to investigate other additives that are clearly distinguished in CLSM images.

Acknowledgements

The authors acknowledge the University of Antwerp for funding the AQ²UABIT (Advanced Qualitative and QUantitative surface Analysis of BITuminous binders using laser scanning confocal microscopy) project with the IOF-SBO research fund (project nr. 40204).

References

[1] Asphalt Institute. The Bitumen Industry: A Global Perspective, Production, Chemistry, Use, Specification and Occupational Exposure. Asphalt Institute Inc. & European Bitumen Association-Eurobitume. (2011).

[2] J.C. Petersen, A review of the fundamentals of asphalt oxidation: chemical, physicochemical, physical property, and durability relationships, Transportation Research Circular. (2009).

[3] P.E. Yuhong Wang, Y. Wen, K. Zhao, D. Chong, A.S.T. Wong, Evolution and locational variation of asphalt binder aging in long-life hot-mix asphalt pavements, Construction and Building Materials. 68 (2014) 172–182. https://doi.org/https://doi.org/10.1016/j.conbuildmat.2014.05.091.

[4] F. Wang, Y. Xiao, P. Cui, J. Lin, M. Li, Z. Chen, Correlation of asphalt performance indicators and aging Degrees: A review, Construction and Building Materials. 250 (2020) 118824. https://doi.org/https://doi.org/10.1016/j.conbuildmat.2020.118824.

[5] G. Pipintakos, H. Soenen, H.Y.V. Ching, C. vande Velde, S. van Doorslaer, F. Lemière, A. Varveri, W. Van den bergh, Exploring the oxidative mechanisms of bitumen after laboratory short- and long-term ageing, Construction and Building Materials. 289 (2021) 123182. https://doi.org/https://doi.org/10.1016/j.conbuildmat.2021.123182.

[6] L.D. Poulikakos, S. dos Santos, M. Bueno, S. Kuentzel, M. Hugener, M.N. Partl, Influence of short and long term aging on chemical, microstructural and macro-mechanical properties of recycled asphalt mixtures, Construction and Building Materials. 51 (2014) 414–423. https://doi.org/https://doi.org/10.1016/j.conbuildmat.2013.11.004.

[7] G. Pipintakos, H.Y. Vincent Ching, H. Soenen, P. Sjövall, U. Mühlich, S. van Doorslaer, A. Varveri, W. Van den bergh, X. Lu, Experimental investigation of the oxidative ageing mechanisms in bitumen, Construction and Building Materials. 260 (2020) 119702. https://doi.org/https://doi.org/10.1016/j.conbuildmat.2020.119702.

[8] M.C. Cavalli, M. Zaumanis, E. Mazza, M.N. Partl, L.D. Poulikakos, Aging effect on rheology and cracking behaviour of reclaimed binder with bio-based rejuvenators, Journal of Cleaner Production. 189 (2018) 88–97. https://doi.org/https://doi.org/10.1016/j.jclepro.2018.03.305.

[9] A.A.A. Molenaar, E.T. Hagos, M.F.C. Van de Ven, Effects of Aging on the Mechanical Characteristics of Bituminous Binders in PAC, Journal of Materials in Civil Engineering. 22 (2010) 779–787. https://doi.org/10.1061/(ASCE)MT.1943-5533.0000021.

[10] A. Rosinger, Beiträge zur Kolloidchemie des Asphalts, Kolloid-Zeitschrift. 15 (1914) 177–179. https://doi.org/10.1007/BF01427821.

[11] D.W. Christensen, D.A. Anderson, Rheological evidence concerning the molecular architecture of asphalt cements, Proc. Chemistry of Bitumen. 2 (1991) 568–595.

[12] O.C. Mullins, H. Sabbah, J. Eyssautier, A.E. Pomerantz, L. Barré, A.B. Andrews, Y. Ruiz-Morales, F. Mostowfi, R. McFarlane, L. Goual, R. Lepkowicz, T. Cooper, J. Orbulescu, R.M. Leblanc, J. Edwards, R.N. Zare, Advances in Asphaltene Science and the Yen–Mullins Model, Energy & Fuels. 26 (2012) 3986–4003. https://doi.org/10.1021/ef300185p.

[13] J. Eyssautier, P. Levitz, D. Espinat, J. Jestin, J. Gummel, I. Grillo, L. Barré, Insight into Asphaltene Nanoaggregate Structure Inferred by Small Angle Neutron and X-ray Scattering, The Journal of Physical Chemistry B. 115 (2011) 6827–6837. https://doi.org/10.1021/jp111468d.

[14] H.R. Fischer, E.C. Dillingh, On the investigation of the bulk microstructure of bitumen - Introducing two new techniques, Fuel. 118 (2014) 365–368. https://doi.org/10.1016/j.fuel.2013.11.008.

[15] Y. Hou, L. Wang, D. Wang, M. Guo, P. Liu, J. Yu, Characterization of bitumen micro-mechanical behaviors using AFM, phase dynamics theory and MD simulation, Materials. 10 (2017). https://doi.org/10.3390/ma10020208.

[16] J. Blom, H. Soenen, A. Katsiki, N. van den Brande, H. Rahier, W. Van den Bergh, Investigation of the bulk and surface microstructure of bitumen by atomic force microscopy, Construction and Building Materials. 177 (2018) 158–169. https://doi.org/10.1016/j.conbuildmat.2018.05.062.

[17] G. Binnig, C.F. Quate, C. Gerber, Atomic force microscope, Physical Review Letters. 56 (1986) 930.

[18] G.D. Danilatos, Mechanisms of detection and imaging in the ESEM, Journal of Microscopy. 160 (1990) 9–19. https://doi.org/https://doi.org/10.1111/j.1365-2818.1990.tb03043.x.
[19] B.V.R. Tata, B. Raj, Confocal laser scanning microscopy: Applications in material science and technology, Bulletin of Materials Science. 21 (1998) 263–278. https://doi.org/10.1007/BF02744951.
[20] H. Fischer, L.D. Poulikakos, J.-P. Planche, P. Das, J. Grenfell, Challenges While Performing AFM on Bitumen BT - Multi-Scale Modeling and Characterization of Infrastructure Materials, in: N. Kringos, B. Birgisson, D. Frost, L. Wang (Eds.), Springer Netherlands, Dordrecht, 2013: pp. 89–98.
[21] S.N. Nahar, A.J.M. Schmets, A. Scarpas, G. Schitter, Temperature and thermal history dependence of the microstructure in bituminous materials, European Polymer Journal. 49 (2013) 1964–1974. https://doi.org/https://doi.org/10.1016/j.eurpolymj.2013.03.027.
[22] S.N. Nahar, A.J.M. Schmets, C. Kasbergen, G. Schitter, A. Scarpas, Self-healing of bituminous materials by damage reversal at the microstructural scale, in: Proceedings of the 94th Annual Meeting of the Transportation Research Board, 2015: pp. 11–15.
[23] J. Blom, H. Soenen, N. van den Brande, W. Van den bergh, New evidence on the origin of 'bee structures' on bitumen and oils, by atomic force microscopy (AFM) and confocal laser scanning microscopy (CLSM), Fuel. 303 (2021) 121265. https://doi.org/https://doi.org/10.1016/j.fuel.2021.121265.
[24] L. Loeber, O. Sutton, J. Morel, J.-M. Valleton, G. Muller, New direct observations of asphalts and asphalt binders by scanning electron microscopy and atomic force microscopy, Journal of Microscopy. 182 (1996) 32–39. https://doi.org/https://doi.org/10.1046/j.1365-2818.1996.134416.x.
[25] A. Jäger, R. Lackner, Ch. Eisenmenger-Sittner, R. Blab, Identification of four material phases in bitumen by atomic force microscopy, Road Materials and Pavement Design. 5 (2004) 9–24. https://doi.org/10.1080/14680629.2004.9689985.
[26] A.T. Pauli, R.W. Grimes, A.G. Beemer, T.F. Turner, J.F. Branthaver, Morphology of asphalts, asphalt fractions and model wax-doped asphalts studied by atomic force microscopy, International Journal of Pavement Engineering. 12 (2011) 291–309. https://doi.org/10.1080/10298436.2011.575942.
[27] H. Soenen, J. Besamusca, H.R. Fischer, L.D. Poulikakos, J.-P. Planche, P.K. Das, N. Kringos, J.R.A. Grenfell, X. Lu, E. Chailleux, Laboratory investigation of bitumen based on round robin DSC and AFM tests, Materials and Structures. 47 (2014) 1205–1220. https://doi.org/10.1617/s11527-013-0123-4.
[28] R. Lamperti, J. Grenfell, C. Sangiorgi, C. Lantieri, G.D. Airey, Influence of waxes on adhesion properties of bituminous binders, Construction and Building Materials. 76 (2015) 404–412. https://doi.org/https://doi.org/10.1016/j.conbuildmat.2014.11.058.
[29] X. Lu, P. Redelius, Effect of bitumen wax on asphalt mixture performance, Construction and Building Materials. 21 (2007) 1961–1970. https://doi.org/https://doi.org/10.1016/j.conbuildmat.2006.05.048.
[30] EN12607-1, Bitumen and bituminous binders. Determination of the resistance to hardening under the influence of heat and air–Part 1: RTFOT method, 2007.
[31] EN14769, Bitumen and Bituminous Binders. Accelerated Long-term Ageing Conditioning by a Pressure Ageing Vessel (PAV), 2012.
[32] H.L. ZHANG, H.C. WANG, J.Y. YU, Effect of aging on morphology of organo-montmorillonite modified bitumen by atomic force microscopy, Journal of Microscopy. 242 (2011) 37–45. https://doi.org/https://doi.org/10.1111/j.1365-2818.2010.03435.x.
[33] A. Chen, G. Liu, Y. Zhao, J. Li, Y. Pan, J. Zhou, Research on the aging and rejuvenation mechanisms of asphalt using atomic force microscopy, Construction and Building Materials. 167 (2018) 177–184. https://doi.org/https://doi.org/10.1016/j.conbuildmat.2018.02.008.
[34] P.K. Das, R. Balieu, N. Kringos, B. Birgisson, On the oxidative ageing mechanism and its effect on asphalt mixtures morphology, Materials and Structures. 48 (2015) 3113–3127. https://doi.org/10.1617/s11527-014-0385-5.
[35] A. Koyun, J. Büchner, M.P. Wistuba, H. Grothe, Rheological, spectroscopic and microscopic assessment of asphalt binder ageing, Road Materials and Pavement Design. (2020) 1–18. https://doi.org/10.1080/14680629.2020.1820891.
[36] J. Redmon, A. Farhadi, YOLOv3: An Incremental Improvement, (2018). http://arxiv.org/abs/1804.02767.

[37] J. Zhu, R. Balieu, X. Lu, N. Kringos, Microstructure evaluation of polymer-modified bitumen by image analysis using two-dimensional fast Fourier transform, Materials and Design. 137 (2018) 164–175. https://doi.org/10.1016/j.matdes.2017.10.023.

[38] G. Pipintakos, N. Hasheminejad, C. Lommaert, A. Bocharova, J. Blom, Application of Atomic Force (AFM), Environmental Scanning Electron (ESEM) and Confocal Laser Scanning Microscopy (CLSM) in bitumen: A review of the ageing effect, Micron. 147 (2021) 103083. https://doi.org/10.1016/j.micron.2021.103083.

[39] A.R. Pathak, M. Pandey, S. Rautaray, Application of Deep Learning for Object Detection, Procedia Computer Science. 132 (2018) 1706–1717. https://doi.org/10.1016/j.procs.2018.05.144.

[40] R. Girshick, J. Donahue, T. Darrell, J. Malik, U.C. Berkeley, J. Malik, Rich feature hierarchies for accurate object detection and semantic segmentation, in: Proceedings of the IEEE Computer Society Conference on Computer Vision and Pattern Recognition, 2014. https://doi.org/10.1109/CVPR.2014.81.

[41] R. Girshick, Fast R-CNN, in: Proceedings of the IEEE International Conference on Computer Vision, 2015: pp. 91–99. https://doi.org/10.1109/ICCV.2015.169.

[42] S. Ren, K. He, R. Girshick, J. Sun, Faster R-CNN: Towards Real-Time Object Detection with Region Proposal Networks Shaoqing, Advances in Neural Information Processing Systems. (2015) 91–99. https://doi.org/10.4324/9780080519340-12.

[43] W. Liu, D. Anguelov, D. Erhan, C. Szegedy, S. Reed, C.-Y. Fu, A.C. Berg, SSD: Single Shot MultiBox Detector, in: Proceedings of the European Conference on Computer Vision, 2016: pp. 21–37. https://doi.org/10.1007/978-3-319-46448-0.

[44] M. Tan, R. Pang, Q. v. Le, EfficientDet: Scalable and efficient object detection, Proceedings of the IEEE Computer Society Conference on Computer Vision and Pattern Recognition. (2020) 10778–10787. https://doi.org/10.1109/CVPR42600.2020.01079.

[45] A. Jäger, R. Lackner, C. Eisenmenger-Sittner, R. Blab, Identification of four material phases in bitumen by atomic force microscopy, Road Materials and Pavement Design. 5 (2004) 9–24. https://doi.org/10.1080/14680629.2004.9689985.

[46] A.A.K.H. Abu-Ein, A novel methodology for digital removal of periodic noise using 2d fast fourier transforms, Contemporary Engineering Sciences. 7 (2014) 103–116. https://doi.org/10.12988/ces.2014.31065.

[47] H. Soenen, P. Redelius, The effect of aromatic interactions on the elasticity of bituminous binders, Rheologica Acta. 53 (2014) 741–754. https://doi.org/10.1007/s00397-014-0792-0.

[48] G. Pipintakos, J. Blom, H. Soenen, W. Van den bergh, Coupling AFM and CLSM to investigate the effect of ageing on the bee structures of bitumen, Micron. 151 (2021) 103149. https://doi.org/10.1016/j.micron.2021.103149.